Optimizing Single Sweep Range and Doppler Processing for FMCW Radar using Inverse Filtering

A.J. de Jong and Ph. van Dorp
Oude Waalsdorperweg 63
2597 AK, Den Haag
The Netherlands

a.j.dejong@fel.tno.nl

ABSTRACT

We discuss range and Doppler processing for FMCW radar using only a single pulse or frequency sweep. The first step is correlation processing, for which the range and Doppler resolution are limited by the ambiguity function. We show that this resolution can be optimized with an additional inverse filtering step. The method is demonstrated for sinusoidal FMCW radar measurements. Several regularized inverse filters were compared and the non-adaptive pseudo inverse filter gave the best results.

1. INTRODUCTION

In this paper we discuss a technique for simultaneously obtaining range and Doppler information with FMCW radar, using only a single pulse or frequency sweep. The single sweep approach contrasts with the multi sweep approach, where the range info is obtained from the pulse delay and the Doppler info from the phase changes in the range cells from pulse to pulse.

An advantage of single sweep processing is that for a given observation time T the unambiguous range is considerably larger than for the multi sweep approach. The reason is that for multi sweep processing, N sweeps of duration T/N are required to obtain a Doppler axis with N different Doppler cells. A disadvantage of single sweep processing is that the range and Doppler resolutions are generally worse, as we discuss in chapter 2. In this paper we focus on the range and Doppler resolutions for single sweep radar, and in chapter 3 we show how these resolutions can be optimized using inverse filtering. The method is applied to actual measurements of a sinusoidal FMCW radar, as discussed in chapter 4.

2. CORRELATION PROCESSING

2.1 Transmitted and received signals

The transmitted signal is an FM signal around a carrier frequency f_c. The phase of the transmitted signal is given by

$$\varphi(t) = \varphi_0 + 2\pi f_c t + \varphi_m(t),$$

and the instantaneous frequency is found as

$$f(t) \equiv \frac{1}{2\pi}\frac{d\varphi}{dt} = f_c + \frac{1}{2\pi}\frac{d\varphi_m}{dt} \equiv f_c + f_m(t).$$

Paper presented at the RTO SET Symposium on "Target Identification and Recognition Using RF Systems", held in Oslo, Norway, 11-13 October 2004, and published in RTO-MP-SET-080.

The boundaries of $f_m(t)$ determine the bandwidth B of the modulation. Ignoring the initial phase φ_0, the complex transmitted signal reads:

$$\psi_T(t) \equiv \exp[i\varphi(t)] = \exp[i\varphi_m(t)]\exp(i2\pi f_c t) \equiv \mu(t)\exp(i2\pi f_c t).$$

It follows that the transmitted signal can be written as a CW signal times a complex envelope $\mu(t)$. We also need an expression for the received signal of a number of targets k at ranges R_k and with radial velocities u_{rk}. We will use the following approximation, holding for most practical cases [1]:

$$\psi_R(t) = \sum_k V_k \mu(t-\tau_k)\exp[i2\pi(f_c+\nu_k)t],$$

where $\tau_k = 2R_k/c$ is the delay and $\nu_k = 2f_c u_{rk}/c$ is the Doppler frequency. The complex factor V_k contains the attenuation and a possible phase shift.

2.2 The ambiguity function

The objective is to extract the amplitude $|V_k|$, the delay τ_k and the Doppler frequency ν_k for each target k from the received signal $\psi_R(t)$. An ideal approach would be to perform such an operation on $\psi_R(t)$ that we arrive at a function of the following form:

$$Z(\tau,\nu) = \sum_k V_k \delta(\tau-\tau_k, \nu-\nu_k).$$

This would be ideal because this function $Z(\tau,\nu)$ shows sharp peaks at $\tau = \tau_k$ and $\nu = \nu_k$ with amplitude $|V_k|$ for all targets k. An attempt to arrive at this ideal $Z(\tau,\nu)$ is to correlate $\psi_R(t)$ with the following reference signal [1]:

$$\psi_F(t,\nu) = \mu(t)\exp[i2\pi(f_c+\nu)t].$$

This results in

$$Z(\tau,\nu) \equiv \int_t \psi_R(t)\psi_F{}^*(t-\tau,\nu)dt = \sum_k V_k \chi(\tau-\tau_k, \nu-\nu_k),$$

where the function $\chi(\tau,\nu)$ is defined as

$$\chi(\tau,\nu) = \int_t \mu(t)\mu^*(t-\tau)\exp(-i2\pi\nu t)dt.$$

The function $\chi(\tau,\nu)$, which is completely determined by the modulation $\mu(t)$, is known as the ambiguity function [3]. In case $\chi(\tau,\nu) = \delta(\tau,\nu)$, correlation processing would be perfect. Indeed for a (quasi) random modulation, the expectation of the ambiguity function is a delta function [1]. This for instance means that correlation processing is ideal for FM radio signals. More generally, the response $Z(\tau,\nu)$ to a collection of point targets k contains a shifted copy $\chi(\tau-\tau_k,\nu-\nu_k)$ for every target k. The range and Doppler resolutions of the targets is described by the sharpness of the central peak at $\chi(0,0)$.

3. OPTIMIZING CORRELATION PROCESSING

3.1 Inverse filtering

The previous chapter may suggest that the ambiguity function $\chi(\tau,\nu)$ gives the ultimate range and Doppler resolution for a given modulation $\mu(t)$. However, correlation processing as described in chapter 2 is only optimal for (quasi) random signals. In this chapter we show how the resolution and the signal to noise ratio of the correlation result $Z(\tau,\nu)$ can be improved using the well-known technique of inverse filtering [4]. We recall the correlation result:

$$Z(\tau,\nu)=\sum_k V_k\,\chi(\tau-\tau_k,\nu-\nu_k)\,.$$

We now interpret $\chi(\tau,\nu)$ as a point spread or blurring function. Because $\chi(\tau,\nu)$ is exactly known from $\mu(t)$, the blurred shape can be focused to a point with an inverse filter derived from $\chi(\tau,\nu)$. The inverse filter is most conveniently described in the Fourier domain, and therefore we introduce the following Fourier transformations:

$$\zeta(p,q)=F_{pq}\{Z(\tau,\nu)\}\,,$$
$$\xi(p,q)=F_{pq}\{\chi(\tau,\nu)\}\,.$$

In the Fourier domain the correlation is given by

$$\zeta(p,q)=\sum_k V_k\,\exp(-ip\tau_k)\exp(-iq\nu_k)\xi(p,q)\,.$$

Note that in this representation the blurring function $\xi(p,q)$ can be taken out of the summation. This suggests elimination of the blurring with the following filtered version of $\zeta(p,q)$:

$$G(p,q)\equiv H(p,q)\zeta(p,q)\equiv\frac{1}{\xi(p,q)}\zeta(p,q)=\sum_k V_k\,\exp(-ip\tau_k)\exp(-iq\nu_k)\,.$$

Here, $H(p,q)$ is the inverse filter, which is the inverse of the Fourier transform of the ambiguity function. Via an inverse Fourier transform we obtain:

$$g(\tau,\nu)=F_{\tau\nu}^{-1}\{G(p,q)\}=\sum_k V_k\,\delta(\tau-\tau_k,\nu-\nu_k)\,.$$

Thus we eventually arrive at the ideal point target response.

3.2 Pseudo inverse filtering

For the application of inverse filtering in practice, regularization of the inverse filter is necessary. One possibility is the pseudo inverse filter [4]:

$$H_P(p,q)=\frac{1}{\xi(p,q)}\,,\qquad \text{for } |\zeta(p,q)|>K\sigma_N,$$
$$H_P(p,q)=0\,,\qquad \text{for } |\zeta(p,q)|<K\sigma_N.$$

Here σ_N is the noise level and $K > 1$ is a threshold parameter. We see that for (p,q) values where $\zeta(p,q)$ does not sufficiently dominate the noise, $H_P(p,q)$ is cleared. This means that for these (p,q) values, $\zeta(p,q)$ does not contribute to the resulting $G(p,q)$ and $g(\tau,\nu)$.

For noisy signals, noise outliers will be more abundant, and this is particularly devastating at (p,q) values where $|\xi(p,q)|$ is very small. The influence of such outliers can be largely suppressed with a non-adaptive approach, where the filter is cleared where $|\xi(p,q)|$ is small rather than $|\zeta(p,q)|$. This leads to the non-adaptive pseudo inverse filter:

$$H_{PN}(p,q) = \frac{1}{\xi(p,q)}, \quad \text{for } |\xi(p,q)| > K',$$
$$H_{PN}(p,q) = 0, \quad \text{for } |\xi(p,q)| < K'.$$

Here K' is a new threshold parameter. Possibly, one can avoid the discontinuities at the edges of the regions where the filter is cleared with the following modification:

$$H_{PN}(p,q) = \frac{\xi^*(p,q)}{|\xi(p,q)|^2 + K'^2}.$$

This can be regarded as a smoothed version of the non-adaptive pseudo inverse filter.

3.3 The Wiener filter

Similar to the pseudo inverse filter is the Wiener filter [4], which is the optimal filter in the sense of minimizing the expected least square error in the resulting $g(\tau,\nu)$:

$$H_W(p,q) = \frac{\xi^*(p,q)}{|\xi(p,q)|^2 + \sigma_N{}^2 / |\zeta(p,q)|^2}.$$

The Wiener filter is also an adaptive filter requiring the estimation of σ_N. One can introduce an artificial threshold parameter by multiplying σ_N with a factor K, leading to a smoothed version of the pseudo inverse filter $H_P(p,q)$.

4. APPLICATION TO SINUSOIDAL FMCW RADAR MEASUREMENTS

4.1 Sinusoidal FMCW radar

We have applied correlation processing and subsequent inverse filtering on actual measurements of a sinusoidal FMCW radar. For this modulation, we have the following transmitted signal [2]:

$$\psi_T(t) = \exp(i2\pi f_c t + ia\cos 2\pi f_m t) = \exp(ia\cos 2\pi f_m t)\exp(i2\pi f_c t),$$

with the following instantaneous frequency:

$$f(t) = \frac{1}{2\pi}\frac{d\varphi}{dt} = f_c - af_m \sin(2\pi f_m t).$$

We see that the instantaneous frequency variation of the transmitted signal is sinusoidal with bandwidth $B = 2af_m$. The ambiguity function is found as

$$\chi(\tau,\nu) = \int_{<T>} \exp[ia(1-\cos 2\pi f_m \tau)\cos 2\pi f_m t - ia \sin 2\pi f_m \tau \sin 2\pi f_m t]\exp(-i2\pi\nu t)dt\,.$$

Here the integral is only carried out over one modulation period $T = 1/f_m$. Normally the delay τ will be small compared to the modulation period T, so that the latter expression can be simplified by a first order approximation of $\sin(2\pi f_m\tau)$ and $\cos(2\pi f_m\tau)$. This leads to

$$\chi(\tau,\nu) \cong \int_{<T>} \exp(-ia2\pi f_m \tau \sin 2\pi f_m t)\exp(-i2\pi\nu t)dt\,.$$

We now borrow the following expression from the theory of Bessel functions:

$$\exp(iz\sin(\theta)) = \sum_{s=-\infty}^{\infty} J_s(z)\exp(is\theta)\,,$$

where s runs over all integers. Substitution in the previous expression gives

$$\chi(\tau,\nu) = \sum_{s=-\infty}^{\infty} J_s(-a2\pi f_m \tau) \int_{<T>} \exp[i2\pi(sf_m - \nu)t]dt\,.$$

For the computation of $Z(\tau,\nu)$ one can freely choose a set of ν values. Choosing $\nu = nf_m$ with integer n, the integral in the latter expression simplifies to δ_{ns} and we get

$$\chi(\tau, nf_m) = J_n(-\pi B\tau) = (-1)^n J_n(\pi B\tau)\,.$$

This ambiguity function is shown in figure 1. The range, which is proportional to τ runs vertically. In this and all following image plots, darker pixels have higher values. The cross section $\chi(\tau,0)$ is described by $J_0(\pi B\tau)$, with its global maximum at $\tau = 0$ and its oscillations along the τ axis. Cross sections for different $\nu = nf_m$ are described by n^{th} order Bessel functions. The general behaviour of $J_n(x)$ for $n \neq 0$ is that $J_n(0) = 0$, and that $J_n(x)$ slowly increases when x approaches n. Around n, it subsequently arrives at its global maximum and first non-trivial zero and then starts oscillating. This explains the bowtie shape of figure 1.

The Fourier transform $\xi(p,q)$ of the ambiguity function $\chi(\tau,\nu)$ is shown in figure 2. The non-adaptive pseudo inverse filter $H_{PN}(p,q)$ following from it is shown in figure 3. Note the interchange of darker and lighter regions between figures 2 and 3, illustrating that figure 3 is the inverse of figure 2. Also note the white regions with sharp edges where $H_{PN}(p,q)$ is cleared because $|\xi(p,q)| < K'$. Figure 4 shows the inverse filter $h_{PN}(\tau,\nu)$ in the range Doppler domain.

4.2 Inverse filtering for actual measurements

We now discuss the application of inverse filtering on measurements of a ground based sinusoidal FMCW radar observing airborne targets. The range and Doppler resolutions are about 1km and 200Hz respectively. Inverse filtering was carried out with $|Z(\tau,\nu)|$ and $|\chi(\tau,\nu)|$, which gave better results than when we worked with $Z(\tau,\nu)$ and $\chi(\tau,\nu)$. We tried the three different regularized filters discussed in chapter 3 and we found that all of them worked very well for targets dominating the noise. Figure 5 shows

$Z(\tau,\nu)$ for a strong target and figure 6 shows the resulting $g(\tau,\nu)$ after successive inverse filtering. We only show one figure, because the different regularized filters performed equally well for this case.

For noisy targets, we expected the non-adaptive pseudo inverse filter to work best. This is illustrated by figures 7-10. Figure 7 shows $Z(\tau,\nu)$ for a weaker target, and figures 8 to 10 show $g(\tau,\nu)$ for $H_{PN}(p,q)$, $H_P(p,q)$ and $H_W(p,q)$ respectively. For the pseudo inverse filter, the value $K = 2$ was chosen. The noise level σ_N was estimated from (p,q) regions where no target contribution to $\zeta(p,q)$ was expected. Clearly, the resulting $g(\tau,\nu)$ is not extremely good for any of the inverse filters, but $H_{PN}(p,q)$ focuses most of the energy in a relatively small region. In addition, the background is smoother, containing fewer outliers.

Figure 11 shows an interesting measurement with 2 targets. The range runs from about 0 to 100km and the Doppler frequency from about –20kHz to 20kHz. Ground clutter is suppressed with a band filter around 0Hz, which is visible as a slight depression in the centre of the figure. The image shows two clear bowtie shapes with different range and different Doppler frequency. Apparently, one target is an incoming target, while the other is an outgoing target. Note that the target on the right hand side of the plot is accompanied by a bowtie at the same range, but with higher Doppler and with lower intensity. This may well be due to JEM (Jet Engine Modulation) of the main target. Figure 12 shows the compression achieved by inverse filtering using $H_{PN}(p,q)$. Figures 13 and 14 show the same information in surface plots.

5. CONCLUSIONS

In the above chapters we discussed the possibilities of optimizing the range and Doppler resolutions of single sweep FMCW radar processing by an additional inverse filtering step after correlation processing. As discussed, the inverse filter can be derived from the ambiguity function of the chosen modulation, and we have given a number of regularized inverse filters for application in practice.

We have demonstrated the technique for actual measurements of a ground based sinusoidal FMCW radar observing airborne targets. We have compared the results of different regularized inverse filters, and found that all filters performed well for targets dominating the noise. For noisy targets the non-adaptive pseudo inverse filter performed best.

For future research it would be interesting to compare the performance of deterministic modulations to (quasi) random modulations. For random modulations, the expectation of the ambiguity function is already a delta function without inverse filtering, but one may expect more noise outliers.

It might be added that after inverse filtering, the range and Doppler resolutions of single sweep processing can in principle be as good as for multi sweep linear FMCW processing. Then, however, the single sweep radar will need a much high sampling frequency, a much larger data buffer and much faster data processing than the multi sweep FMCW radar. Instead, one will rather use single sweep radar for its potential of a large unambiguous range and Doppler frequency, while the observation time can be short.

6. REFERENCES

[1] R.L. Mitchell, *Radar Signal Simulation* (1976).
[2] M. Skolnik, *Introduction to Radar Systems* (1981).
[3] S.M. Sussman, *Least Square Synthesis of Radar Ambiguity Functions*, Trans. IRE, vol. IT-8, 246-54 (1968).
[4] M. Schwartz. L. Shaw, *Signal Processing* (1975).

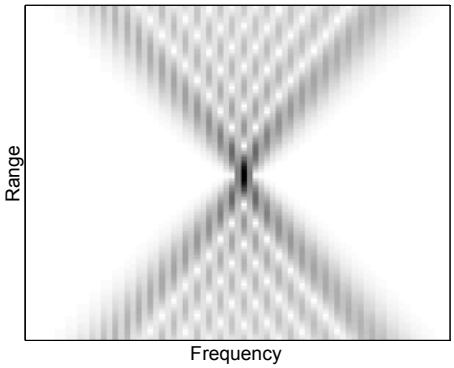

Figure 1: Modulus of the ambiguity function $\chi(\tau,\nu)$. The centre of the plot is $\chi(0,0)$.

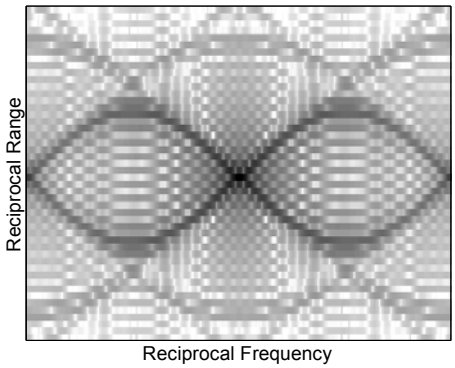

Figure 2: Modulus of $\xi(p,q)$. The centre of the plot is $\xi(0,0)$.

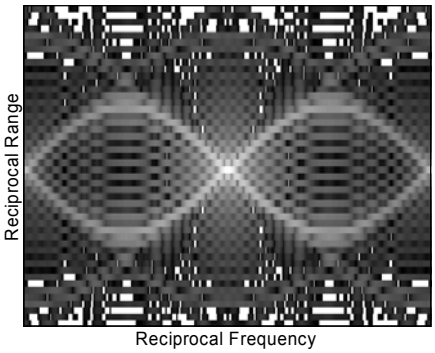

Figure 3: Modulus of $H_{PN}(p,q)$. The centre of the plot is $H_{PN}(0,0)$.

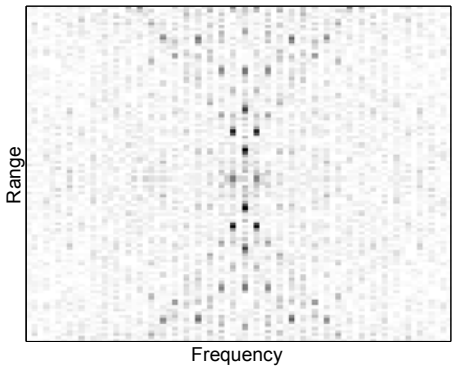

Figure 4: Modulus of $h_{PN}(\tau,\nu)$. The centre of the plot is $h_{PN}(0,0)$.

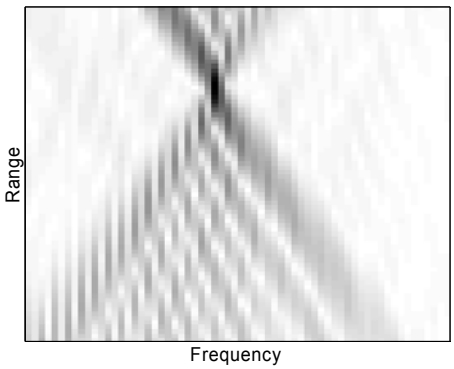

Figure 5: Modulus of $Z(\tau,\nu)$ for a strong target.

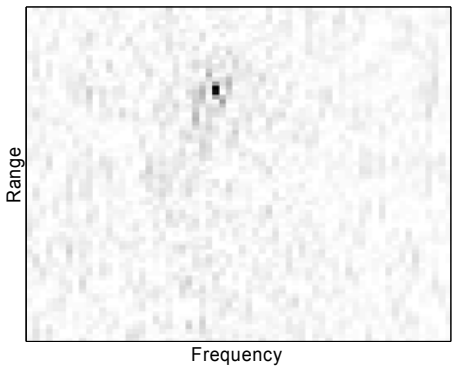

Figure 6: Modulus of $g(\tau,\nu)$ for the target of figure 5.

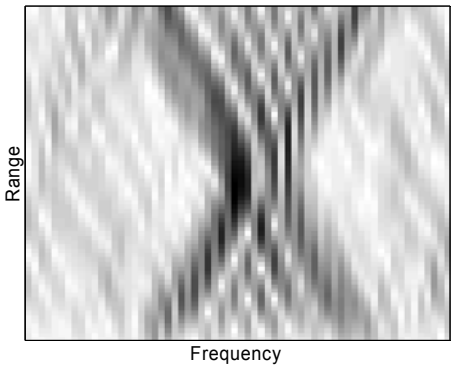

Figure 7: Modulus of $Z(\tau,\nu)$ for a weak target.

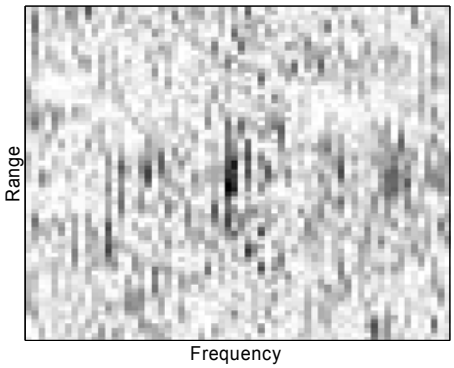

Figure 8: Modulus of $g_{PN}(\tau,\nu)$ for the target of figure 7.

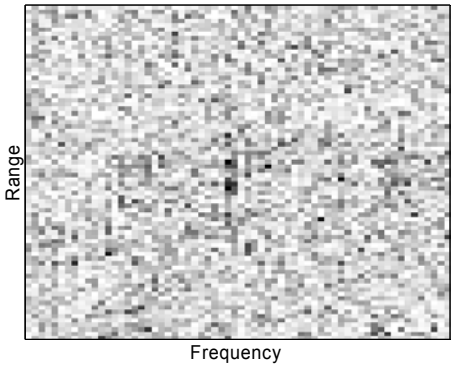

Figure 9: Modulus of $g_{P}(\tau,\nu)$ for the target of figure 7.

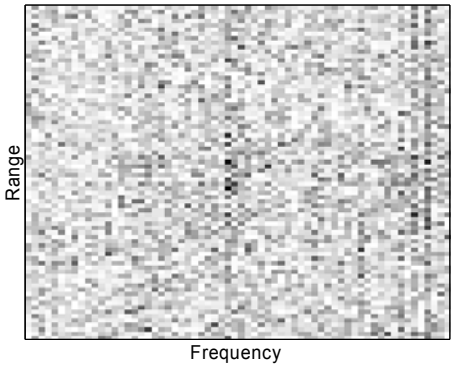

Figure 10: Modulus of $g_{W}(\tau,\nu)$ for the target of figure 7.

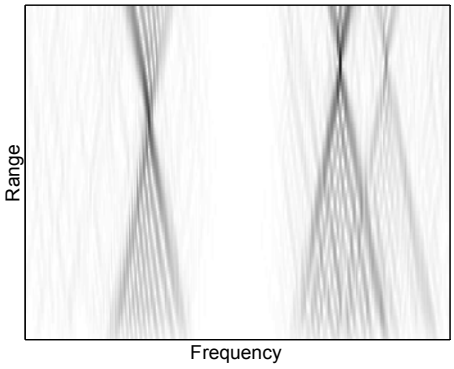

Figure 11: Modulus of $Z(\tau,\nu)$ for a case of multiple targets.

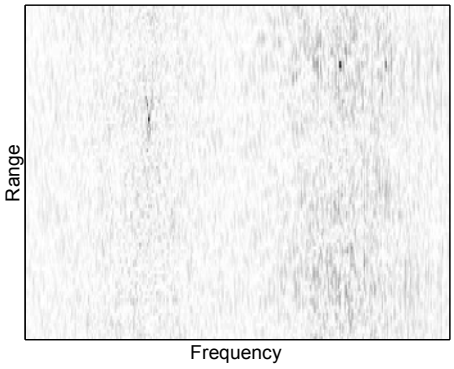

Figure 12: Modulus of $g_{PN}(\tau,\nu)$ corresponding to figure 11.

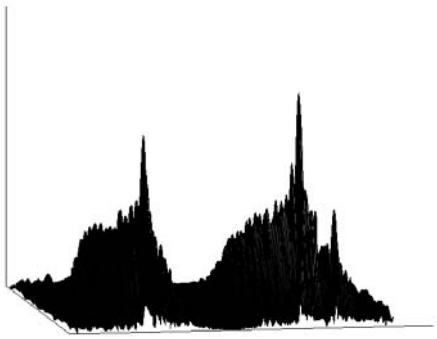

Figure 13: Surface plot corresponding to figure 11. The range axis points towards the reader.

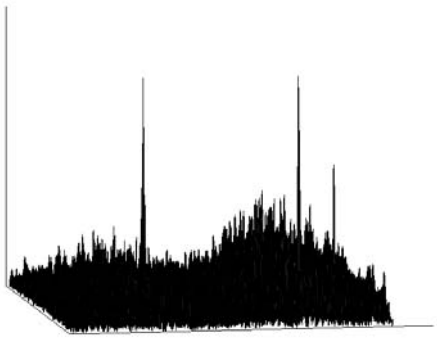

Figure 14: Surface plot corresponding to figure 12. The range axis points towards the reader.